Structural Evolution: Mechanism of Olefin Insertion in Hydroformylation Reaction

Juan P. Salinas-Olvera,[†] Rosa M. Gómez,[‡] and Fernando Cortés-Guzmán*,[†]

Facultad de Química, Departamento de Química Orgánica, Universidad Nacional Autónoma de México, México D.F., 04510, México, and Facultad de Química, Departamento de Química Inórganica y Organometálica, Universidad Autónoma del Estado de México, Toluca, Estado de Méxco, 50120, México

Received: November 26, 2007; In Final Form: January 3, 2008

Hydroformylation is the transformation of an alkene to an aldehyde via the addition of both hydrogen and carbon monoxide. The final aldehyde has one more carbon atom than the precursor alkene. Two isomeric products can result. The regiochemistry of the hydroformylation reaction is believed to be controlled by the olefin insertion step. A reaction mechanism is usually studied by finding the reactants, products, intermediates, and transition states. Alternatively, a chemical reaction can be studied from the redistribution of the electron density along the reaction path connecting the stationary points. The aim of this work is to describe the reaction mechanism of the insertion process by the structural evolution defined by the changes in the electron density during the reaction.

Introduction

Hydroformylation is the transformation of an alkene to an aldehyde via the addition of both hydrogen (H_2) and carbon monoxide (CO). The final aldehyde has one more carbon atom than the precursor alkene (Scheme 1). The process typically involves high pressure (between 10 and 100 atm) and temperature between 40 and 300 °C. The process requires transition metal catalysts, which typically contain cobalt or rhodium. A key consideration of hydroformylation is the normal vs iso selectivity. The issue is illustrated in the hydroformylation of propene. Two isomeric products can result: butyraldehyde or isobutyraldehyde. These isomers result from the differing ways of inserting the alkene into the M−H bond. Of course, both products are not equally desirable. Much research has been dedicated to the quest for catalyst that favored the normal isomer.

Heck and Breslow first proposed a mechanism for cobalt-based hydroformylation process in 1961.[1] The catalytic cycle consists of five elementary reaction steps: (1) CO dissociation, (2) olefin coordination, (3) olefin insertion and CO addition, (4) CO insertion, and (5) H_2 oxidative addition and aldehyde reductive elimination.

The regiochemistry of the hydroformylation reaction is believed to be controlled by the olefin insertion step that converts the L_nMH(alkene) complex into the linear or branched L_nM-(alkyl) structure. The L_nMH(alkene) species has never been observed directly, presumably due to its reactivity. A considerable amount of theoretical work has been reported about hydroformylation. Many theoretical aspects of reactions promoted by $HCo(CO)_4$, have been examined by several groups.[2−6]

Structure, Stability, Change, and Evolution. The classical approach toward the determination of a reaction mechanism is based in the evolution of the energy along the reaction, where the potential energy profile associated with the reaction pathway connecting the stationary points−reactants, products, intermediates, and transition states−is obtained. By means of the characterization of these stationary points on the potential energy surface for a similar set of reactions, chemical trends can be deduced. Alternatively, a chemical reaction can be studied from the redistribution of the electron density along the reaction path connecting the stationary points. It is possible to understand the bond breaking/forming processes in a reaction. Bader and co-workers pioneered the study of the structural change based in the electron density using the Thom's theory of elementary catastrophes.[7] Silvi and co-workers developed the bonding evolution theory as a generalization of the Bader's work to others scalar fields as ELF.[8,9] Several research groups have used the electron density,[10−15] its laplacian,[16] ELF,[17−20] and electrostatic potential[21] to study reaction mechanisms or conformational changes of several systems using these approaches.

SCHEME 1: Hydroformylation Reaction

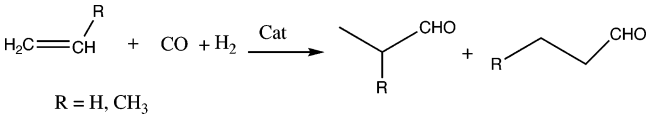

The geometry of a molecular system is defined as the set of nuclear coordinates, denoted collectively by **R**, determining the exact position in space of the all nuclei. Any infinitesimal change in coordinate values leads a different geometry (**R′**). For any configuration **R** there is a charge density $\rho(\mathbf{r},\mathbf{R})$ and its associated gradient vector field $\nabla\rho(\mathbf{r},\mathbf{R})$. This field includes the trajectories that both originate and terminate at the critical points (CP) found between nuclei that appear linked by a saddle in $\rho(\mathbf{r})$. A CP denotes an extremum in $\rho(\mathbf{r})$, a point where $\nabla\rho(\mathbf{r}) = 0$. There are two sets of trajectories associated with a CP between two nuclei called a bond critical point (BCP). A set that starts at infinity and terminate at the BCP defines a surface that separates the basins of neighboring atoms. Also there is a unique pair of trajectories that originate at each such BCP and terminate, one each, at the neighboring nuclei and defines the line of maximum density. In equilibrium geometry the line of maximum density is called a bond path (BP). Thus a line along which the electron density, the glue of chemistry, is maximally concentrated links pairs of bonded atoms. The presence of a

* To whom correspondence should be addressed. E-mail: fercor@servidor.unam.mx.
[†] Universidad Nacional Autónoma de México.
[‡] Universidad Autónoma del Estado de México.

10.1021/jp711200n CCC: $40.75 © 2008 American Chemical Society
Published on Web 02/28/2008

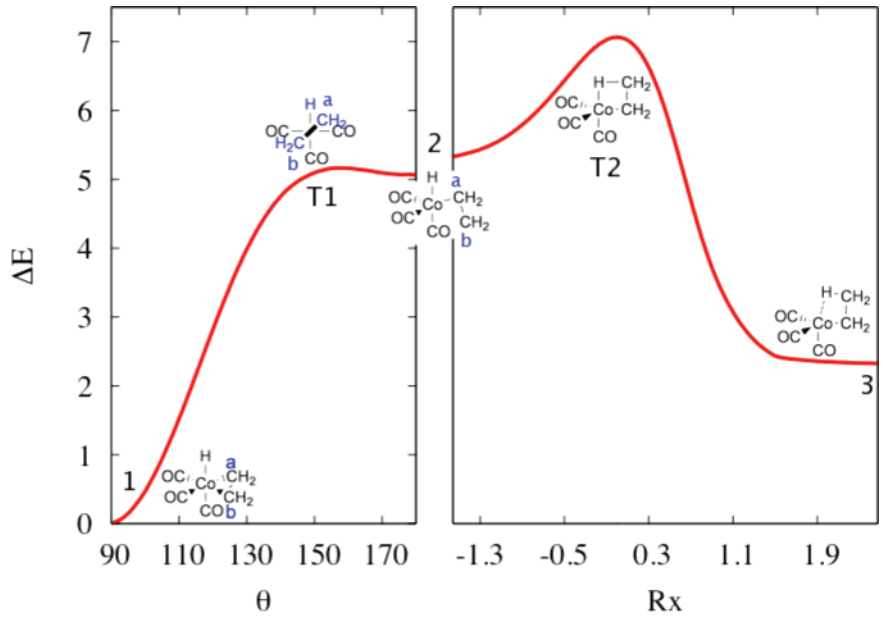

Figure 1. Energy profile of the ethylene insertion. Left, rotation process. Right insertion process.

bond path provides a universal indicator of bonding between the atoms.[22,23] The molecular structure is a connectivity scheme governed by the topology of $\rho(\mathbf{r})$. A molecular graph (MG) is defined as the set of bond paths and CPs. Any configuration of the nuclei $\mathbf{R}'$ in the neighborhood of a given configuration $\mathbf{R}$, while it has a different geometry, should possess the same structure, that is, the same nuclei should be linked by the same network of bond paths in both $\mathbf{R}$ and $\mathbf{R}'$; they have the same connectivity. If two molecular graphs can be continuously mapped into each other (one by one) they are homeomorphic or topologically equivalent. The molecular graph undergoes discontinuous and abrupt changes if the nuclei are displaced into critical configurations. When this occurs, one makes or breaks bonds and changes one structure into another. There are only two types of structural change possible: the bifurcation mechanism and the conflict mechanism, each possessing a corresponding unstable structure. In the bifurcation mechanism a BCP and a ring critical point (RCP) annihilate. The conflict consists of two nuclei competing for a single BP and can be resolved by an infinitesimal distortion of the conflict geometry. The structural change occurs by a structural catastrophe in an unstable structure.

Even the energetic behavior is determined by the structure, the functional that relates the energy to the density, that would enable a complete understanding the energetic and structural changes; it is unknown at this time. There is no a priori reason to expect that a maximum in an energy profile should coincide with a structural catastrophe. For example, Hernández-Trujillo and co-workers reported a Be^{2+}−benzene complex, for which the global minimum is close to a structural catastrophe.[24]

Structural evolution of a chemical reaction may be defined as the study along the chemical reaction mechanism partitioning of nuclear configuration space into a finite number of structural regions using the topology of a scalar field to define structure. In this approach, it is possible to define the sequence of bond breaking and bond formation in a reaction mechanism. The aim of this work is to describe the reaction mechanism of the insertion process by the structural evolution defined by the changes in the electron density during the reaction.

Computational Methods

Geometries were optimized using the 6-311++G(2d,2p) basis set in a calculation using the B3LYP methods given in GAUSSIAN 03.[25] This method has usefully reproduced experimental behavior of cobalt complexes.[6] The frequency calculations were carried out at same theoretical level to confirm ground (NImag=0) and transition (NImag=1) states. The IRC was followed at the same theoretical level. The BCP properties were calculated using AIMAll97.[26] The programs AIM2000[27] and AIMPAC[28] have been used in the construction of the diagrams.

Results and Discussion

The olefin insertion is preceded by the olefin coordination to $HCo(CO)_3$, which is in a planar C_{2v} singlet state with the hydrogen along the C_2 axis,[6] to yield a complex with the olefin perpendicular to the axial Co−H bond. This is the olefin orientation of higher stability in the complex.[29−32]

The insertion process consists of two steps: the first one is an olefin rotation from the perpendicular toward the parallel orientation to the Co−H bond. The second one is the migration of the hydrogen from the cobalt to the carbon atom to produce the alkyl−Co complex. Alagona and co-workers studied the potential energy for the rotation of the H−Rh−C═C dihedral with several olefins using a flexible rotor approximation. They found, for all cases, a deep minima when the H−Rh bond is perpendicular to the C═C bond, whereas there is a shallow local minima when the H−Rh bond is parallel to it.[31] Ziegler and co-worker related the stability of the perpendicular conformation with a stronger back-bonding component in that orientation.[29]

Ethylene. Figure 1 shows select parts of the energy profile of the ethylene insertion process. The first step is an olefin rotation of 90°, from a perpendicular arrangement with respect to the Co−H bond (**1**, H−Co−C(a)−C(b) = 90.9°) toward a parallel orientation (**2**, H−Co−C(a)−C(b) = 179.2°), 5.06 kcal/mol less stable. The barrier of this process (**T1**) is of 5.16 kcal/mol and presents a dihedral of 157.3°. In the second step, the olefin insertion takes place with a barrier (**T2**) of 1.73 kcal/mol, the H atom migrates from the Co to the C(a). Finally, **3**, the product of insertion is a tetracoordinate complex $(CO)_3Co-CH_2CH_3$, 2.3 kcal/mol less stable than the initial structure **1**.

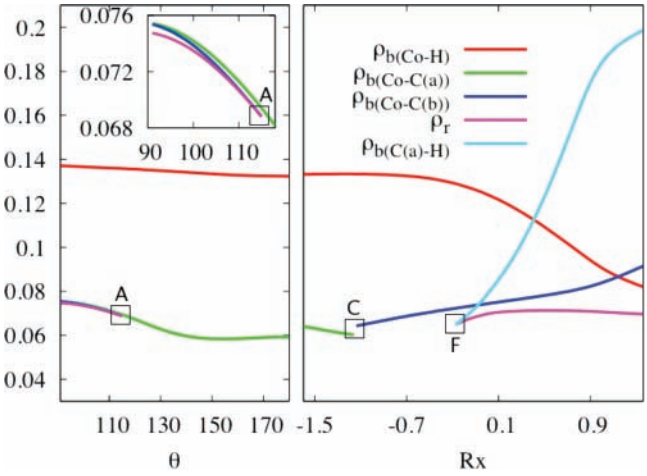

Figure 2. Bond path evolution in the ethylene insertion. Left, rotation process. Right, insertion process. ρ_b, density at the BCP. ρ_r, density at RCP.

Figure 2 shows the evolution of the electron density of selected BCPs during the rotation and insertion processes. Figure 3 presents the MG of selected structures in the evolution of the reaction. The MG of **1** shows a ring formed by two Co−C bond paths and one C−C bond path. It is characterized by a RCP. This structure agrees with the expected η^2 complex. The small values of ρ_b for the bonded interactions with Co (0.136 for Co−H and 0.075 for Co−C) are typical of bonding to a transition metal atom (M). Bonding to M is also characterized by small values for $|H_b|$ (−0.072 for Co−H and −0.018 for Co−C). The total energy density can be defined as $H_b = G_b + V_b$ where the potential energy density at the BCP is V_b (always negative) and kinetic energy density at a BCP is G_b (always positive). In a BCP of covalent bonds, V_b is dominating, and thus H_b is negative at the BCP. On the other hand, the excess of kinetic energy provokes H_b to be positive. The small values of ρ_b and $|H_b|$ result from the BCP for the M−ligand interaction falling in the outer shell of charge depletion of the metal atom, the region where $\nabla^2\rho > 0$ (0.078 for Co−H and 0.075 for Co−C). The C−C bond is a classical shared shell interaction in both the isolated ($\rho_b = 0.344$, $\nabla^2\rho_b = -1.028$, $H_b = -0.395$) and coordinated olefins ($\rho_b = 0.309$, $\nabla^2\rho_b = -0.845$, $H_b = -0.320$), but this shared shell feature decreases in the complex. The values of ρ_r (ρ at a RCP) is slightly smaller (0.074) than ρ_b for the peripheral Co−C bonds. Because the electronic charge is concentrated to an appreciable extent over the entire surface of a three-member ring, the rate of the falloff in the charge density from its maximum value along the bond path toward the interior of the ring is much lower than its rate of decline in the directions perpendicular to the ring surface. At the BCP the electron density is a minimum along the line linking both atoms and maxima in the remaining two normal directions. Ellipticity, ϵ, is defined as $\epsilon = \lambda_1/\lambda_2 - 1$, where λ_1 and λ_2 are the negative eigenvalues of the Hessian of the electron density at the BCP, ordered such that $\lambda_1 < \lambda_2 < 0 < \lambda_3$. The ellipticity can be interpreted as a measure of the anisotropy of the curvature of the electron density in the directions normal to the bond.[33] Both Co−C bonds have substantial ellipticities, 2.865, and their major axes lie in the plane of the ring. A significant bond ellipticity of the Co−C, $\epsilon > 1$, indicates that the bond path is susceptible to rupture by a suitable change in the geometry.

In Figures 2 and 3, it is possible to observe three structural changes, one in the rotation process and two in the insertion process. The rotation produces a structural change catastrophe; the opening of the ring structure occurs by a bifurcation when the RCP, the point of lowest density in the ring surface, coalesces with a BCP of the three-membered ring, the point of lowest density along the bond path. At **1**, the RCP is 0.24 Å from both Co−C BCPs. Increasing the dihedral H−Co−C(a)−C(b), the RCP approaches to the Co−C(b) BCP. At 116°, the RCP−BCP distance is 0.04 Å. The catastrophe occurs at 117° (A in Figure 3); after this angle the Co−C(b) bond path is no longer present, and the complex is not a η^2 anymore. Figure 4 shows the change of the ellipticity in the three catastrophes. The ellipticity of the Co−C(b) BCP increase from 2.86 to a maximum in 59.02 before the first catasatrophe. The rotation process presents a transition state **T1**, at 157.3°, and finishes in **2**, at 179.2°. The rotation process produces a geometry change of the complex from square bipyramid to trigonal bipyramid. There is an opening of the equatorial CO angle. The angle between the Co and the equatorial CO ligands shows a value of 118.6° in **1**, with an increase of 12.6° in **T1**. In **2** the angle is 133.5°.

Through the reaction path from **2** to **T2**, a structural catastrophe by a conflict mechanism occurs (part C in Figure 3). There is a migration of the bond path from Co−C(a) to Co−C(b) (parts B and D in Figure 3). The ellipticity of the Co−C(a) increases from 5.46 to 77.68 before the catastrophe. Both λ_1 and λ_2 increase, but the change of λ_1 is faster. This catastrophe approaches the C(a) to the hydride. Figure 5 shows the laplacian envelope of this structure. It is possible to observe an charge depletion (CD) on the C(a), (arrow in Figure 5), oriented to the hydride, associated with a charge concentration (CC). The complementary mapping of the regions of CC and CD determines the donor−acceptor interactions of transition metal complexes.[23,34] This CC−CD (key−lock) relationship in the laplacian predicts the future of the change in this structure, forming a ring with a new H−C(a) bond.

In **T2** a ring is formed by the H, Co, C(b), and C(a) atoms and a ring critical point is observed. This structure is formed before **T2** by a bifurcation catastrophe where the H−C(a) BCP and a RCP appear (E in Figure 3). After that point the density of the H−C(a) increases and the one of Co−H BCP decreases. This process is characterized by a decrease of the H−C(a) BCP ellipticity from 1.61 to 0.04 (Figure 4). Along the rest of the IRC the RCP moves closer to the Co−H BCP. If **3** were not an energetically stable structure, one would expect to observe another bifurcation catastrophe where the Co−H BCP and the RCP annihilate. **3** presents a Co···H−C agostic (which commonly refers to a C−H bond on a ligand that undergoes an interaction with the metal complex) interaction at the formally vacant axial position. It has been assumed that this interaction stabilizes the intermediary.[30] But the Co···H−C interaction is present since the four-membered ring formation. From Figures 1 and 2, it is possible to relate the stability of **3** to the decrease of the density at the Co−H interaction and the increase of the density at the H−C(a) interaction.

The mechanism of the ethylene insertion in the Co−H bond can be described with two energetic steps and three structural changes. The first energetic step has a bifurcation catastrophe that breaks the Co−C−C three-membered ring. The second one has two structural changes: a conflict that transposes a Co−C bond and bifurcation catastrophes that forms a Co−C−C−H four-membered ring. This ring produces the migration of the hydride from the cobalt atom to the carbon atom.

Propene. The reaction mechanism described above appears to be general for symmetric olefins. However, asymmetric olefins have some differences that will be shown below. The butanal/2-metilpropanal ratio of the produced aldehydes, in the

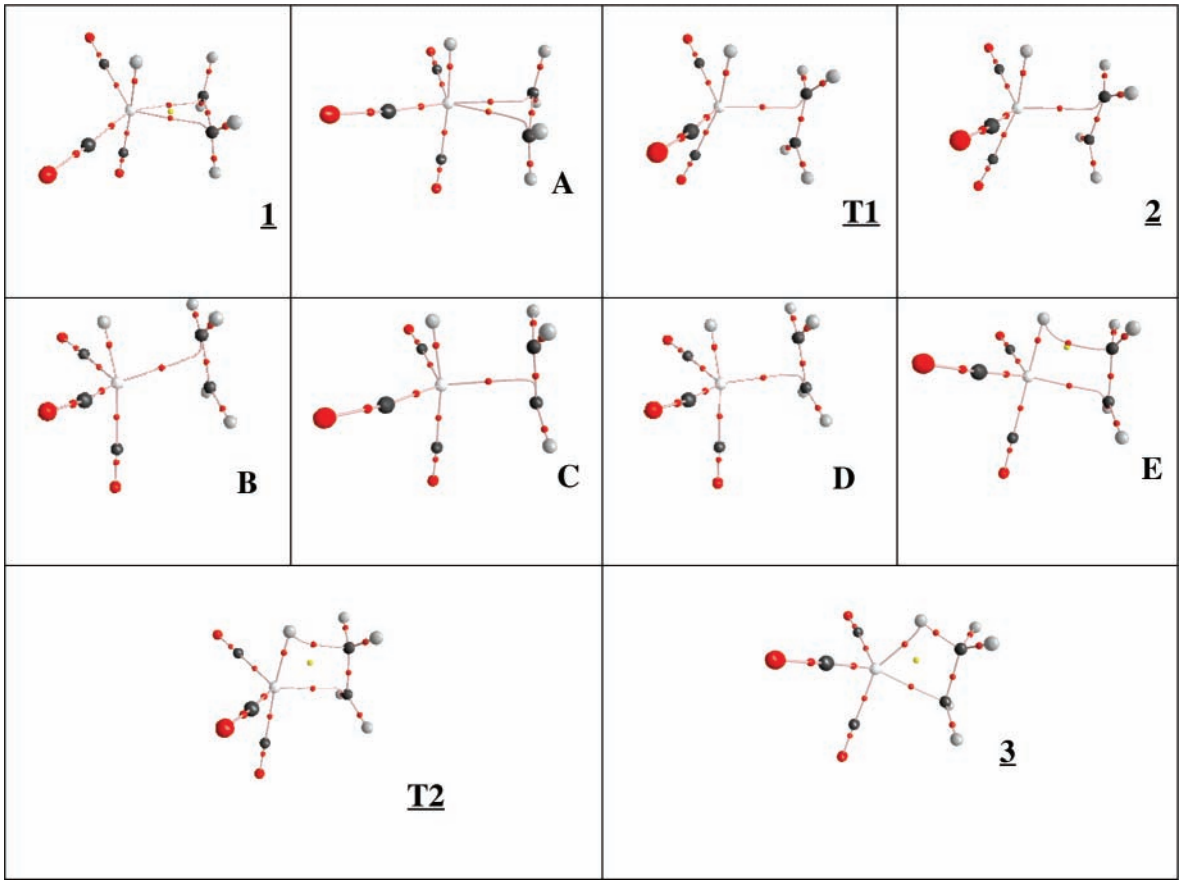

Figure 3. Molecular graphs involved in the insertion mechanism of ethylene.

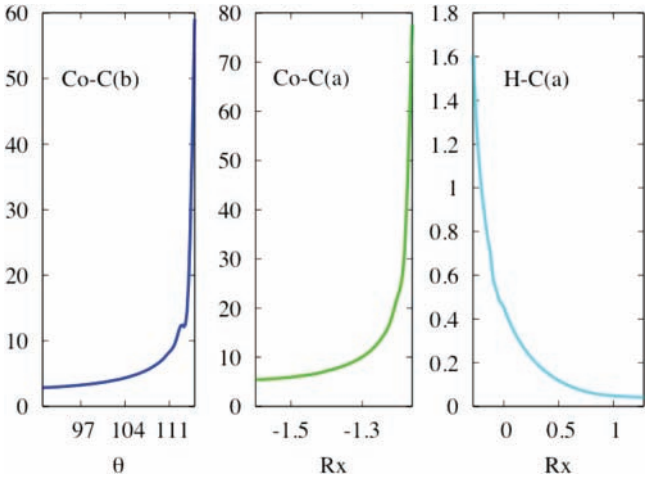

Figure 4. Evolution of the ellipticity in the three catastrophes of the ethylene insertion.

propene hydroformylation, is 4:1 for experiments without ligands.[35] The mechanism of the formation of each aldehyde, normal and iso, has different structural evolutions.

Figure 6 shows selected parts of the energy profile of the propene insertion process. The first step is a rotation of 90°, from the complex **1′** (Figure 7) with perpendicular arrangement with respect to the Co−H bond toward a parallel orientation where two conformers are possible: methyl group at the same side as in (**2′-*syn***) or at the opposite side from of (**2′-*anti***) the Co−H bond. The anti rotation shows a continuous increase of energy, the **2′-*anti*** conformer is 4.4 kcal/mol less stable than the perpendicular conformer. The syn rotation shows a barrier of 4.6 kcal/mol. The **2′-*syn*** conformer is 4.2 kcal/mol less stable than the perpendicular conformer. The second part of the

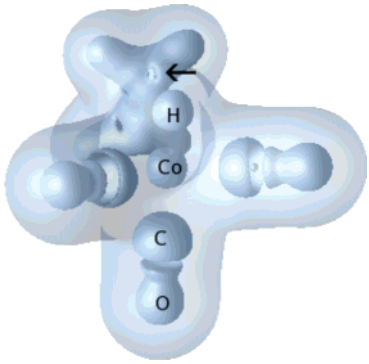

Figure 5. Zero envelope of the laplacian (inner) and the 0.001 density envelope (outer) of **D** complex.

insertion process is the hydride migration. The **2′-*syn*** conformer produces the lineal product by an anti-Markovnikov insertion, while the **2′-*anti*** conformer is transformed by a Markovnikov insertion to the branched product. The former process has a barrier of 2.46 kcal/mol and the latter has a barrier of 2.8 kcal/mol. The final products of the insertion reaction have a energy difference of 0.45 kcal/mol.

The perpendicular conformer is not a η^2 structure. Figure 7 shows the MG of **1′** where the Co−CH_2 BP is present, while the Co−CH BP and the ring structure are not. The bond distances of Co−CH_2 and Co−CH are 2.150 and 2.192 Å, respectively. The properties of the Co−CH_2 BCP are $\rho_b = 0.073$, $\nabla^2\rho_b = 0.180$, $\epsilon = 1.534$, $H_b = -0.019$; the C−C BCP properties are $\rho_b = 0.318$, $\nabla^2\rho_b = -0.920$, $\epsilon = 0.222$, $H_b = -0.339$, and the Co−H BCP properties are $\rho_b = 0.137$, $\nabla^2\rho_b = 0.079$, $\epsilon = 0.037$, $H_b = -0.044$. These values are very similar to the same interaction in the ethylene case.

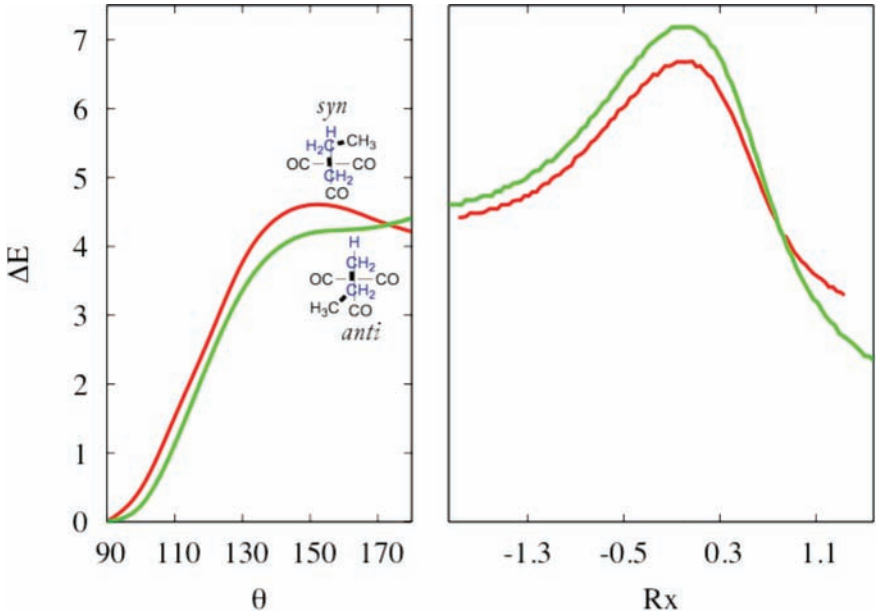

Figure 6. Energy profile of propene insertion. Left, rotation process. Right, insertion process.

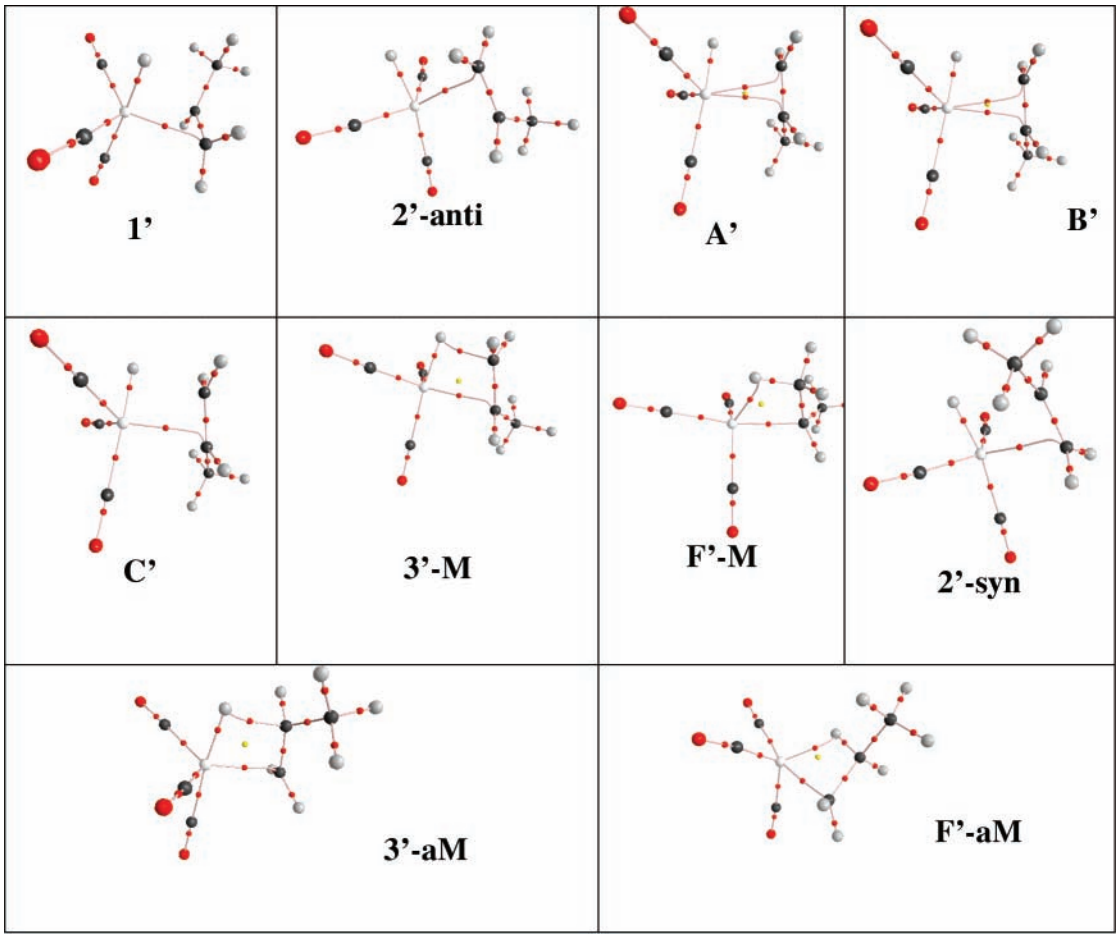

Figure 7. Molecular graphs involved in the insertion mechanism of propene.

Parts a and b of Figure 8show the evolution of the bond path for the insertion process for Markovnikov and anti-Markovnikov addition reactions. No structural changes along rotation are observed; the **2′-*syn*** and **2′-*anti*** conformers have the same connectivity as **1′** during the rotation. The second process, the hydride migration, presents different structural changes for each type of addition.

Conformer **2′-*syn*** presents a ring formation as the unique structural change. Figure 8a shows a bifurcation catastrophe where a H−CH_2 BCP appears with a RCP to form a ring migration, **3′**-aM (Figure 7). After this catastrophe point the density of the H−CH_2 BCP increases. While the density of the RCP seems to be constant, the density at Co−H BCP decreases getting closer to the RCP.

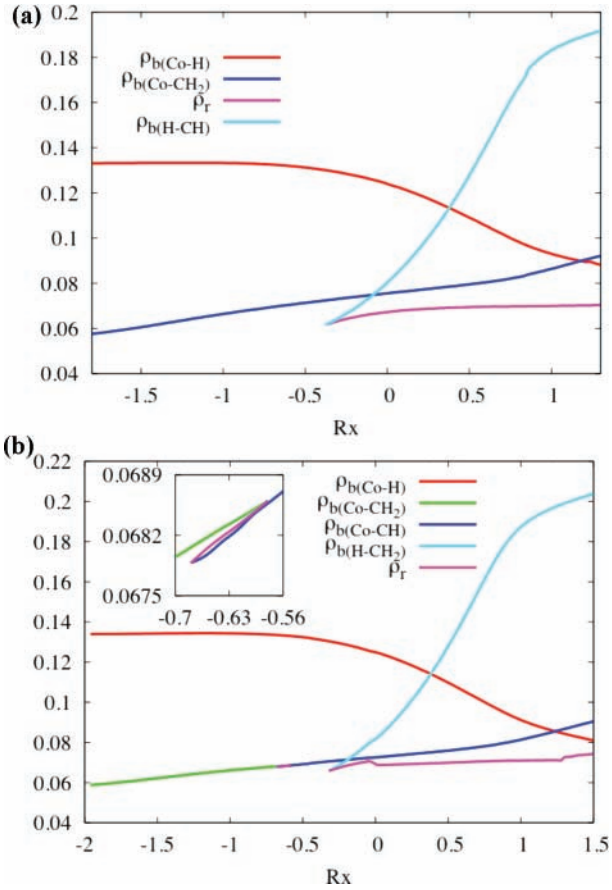

Figure 8. Bond path evolution in the propene insertion. (a) anti-Markovnikov insetion (up). (b) Markovnikov insetion (down). ρ_b, density at the BCP. ρ_r, density at RCP.

The conformer **2′-*anti*** needs two previous structural changes before the system can build the migration ring, **3′**-M (Figure 7). Figure 8b shows a bifurcation catastrophe where a Co−CH BCP appears with a RCP (**A′** in Figure 7). After this catastrophe point, the density of the H−CH_2 BCP increases, while the density of the RCP appears to be constant, and the density of the Co−CH_2 decreases until a new bifurcation catastrophe occurs (**B′** and **C′** in Figure 7). The sequence of two bifurcation catastrophes is equivalent to a conflict catastrophe where a migration of the bond path from Co−CH_2 to Co−CH occurs as in the ethane insertion. The density at the region between the Co and the two carbon atoms is flat, and it allows the structural changes. After this structural change a new bifurcation catastrophe forms the H migration ring, **3′**-M.

The migration rings in both cases undergo a rotation of the Co(CO)3 group producing a cobalt complex with a Co−H interaction at the equatorial and the Co−C bond at the axial positions (**F′-M** and **F′-aM** at Figure 7). The rotation of the Co(CO)3 group does not affect the connectivity. The properties of the Co−H BCP are $\rho_b = 0.061$, $\nabla^2\rho_b = 0.228$, $\epsilon = 0.957$, $H_b = -0.075$, and $\rho_b = 0.062$, $\nabla^2\rho_b = 0.235$, $\epsilon = 1.088$, $H_b = -0.075$ for **F′-aM** and **F′-M**, respectively. The Co−H interaction is slightly stronger in the **F′-M** that produces the branched product.

Figure 9 shows the laplacian envelopes of **C′** and **2′-*syn*** structures, which originate each migration ring. It is possible to observe CDs on the CH_2 (**C′**) and CH (**2′-*syn***) (arrows in Figure 9), oriented toward the hydride, associated with a CC. Each CD can be characterized by a (3,+1) CP at the laplacian scalar field. The (3,+1) CP at CH_2 (**C′**) presents $\nabla^2\rho_{CD} = 0.0314$ and $\rho_{CD} = 0.1669$. This CP is at 1.020 au. from the carbon atom. At CH (**2′-*syn***), the (3,+1) CP has $\nabla^2\rho_{CD} = 0.0171$ and $\rho_{CD} = 0.1543$. The distance from the carbon atom to (3,+1) CP is 1.032 au. The CD at the **2′-*syn*** structure presents 0.0126 au. less density than the CD at **C′**. The CD at **2′-*syn*** is a more electrophilic site than CD at **C′**.

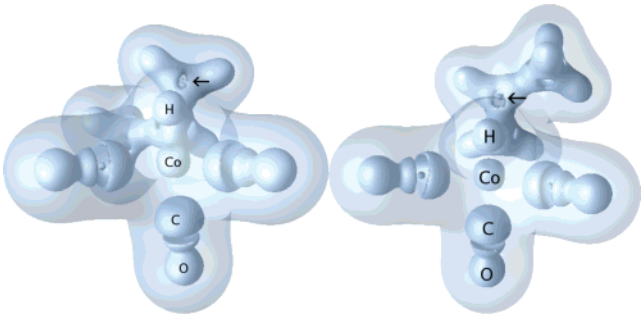

Figure 9. Zero envelope of the laplacian (inner) and the 0.001 density envelope (outer) of **C′** (left) and **2′-*syn*** (right) complexes.

The mechanism of the propene insertion in the Co−H bond can be described according to the type of addition. The Markovnikov addition that produces the branched product presents just one energetic barrier, that of migration, and presents three structural changes by bifurcation catastrophes. The first two changes are equivalent to a conflict catastrophe where a migration occurs of the bond path from Co−CH_2 to Co−CH. The anti-Markovnikov addition that produces the lineal product presents two energetic barriers, one of the rotation process and one of the migration, and presents a ring formation as the unique structural change.

Conclusions

A reaction mechanism consists of two parts: the energetic and the structural evolutions. Every change in the electron density produces an energetic change or vice versa. The energy evolution describes reactants, products, intermediates, transition states, and the paths connecting them. The structure evolution defines the sequence of bond breaking and bond formation in a reaction mechanism by finding the structural catastrophes. In general there is not agreement between a catastrophe and a transition state.

The mechanism of the ethylene insertion in the Co−H bond can be described with two energetic steps and three structural changes. The first energetic step has a bifurcation catastrophe that breaks the Co−C−C three-membered ring. The second one has two structural changes: a conflict that transposes a Co−C bond and bifurcation catastrophes that forms a Co−C−C−H four-membered ring. This ring produces the migration of the hydride from the cobalt atom to the carbon atom

The mechanism of the propene insertion in the Co−H bond can be described according to the type of addition. The Markovnikov addition that produces the branched product presents just one energetic barrier, that of migration, and presents three structural changes by bifurcation catastrophe. The first two changes are equivalent to a conflict catastrophe where occurs a migration of the bond path from Co−CH_2 to Co−CH. The anti-Markovnikov addition that produces the lineal product present two energetic barriers, one of the rotation process and one of the migration, and presents a ring formation as the unique structural change.

The study of the structural evolution of the rest of the reactions of the hydroformylation process is in progress, as well as the study of the evolution of the atomic properties during the reactions.

Acknowledgment. We wish to thank the financial support of UNAM (PAPIIT: IN216205, IN207107, and IN500107), UAEM (SIyEA 1923), and CONACyT (52619). We also thank UNAM-DGSCA for computer time and Dr. J. Hernández and Dr. G. Cuevas for their helpful comments.

Note Added after Print Publication. In the fifth paragraph of the Introduction, the deltas (Δ) should have been nablas (∇). This Article was published on the Web on February 28, 2008 (ASAP) and in the April 3, 2008 issue (Vol. 112, No. 13, pp 2906−2912). The corrected electronic version was posted on May 2, 2008, and an Addition and Correction appears in the May 29, 2008 issue (Vol. 112, No. 21).

References and Notes

(1) Heck, R. F.; Breslow, D. S. *J. Am. Chem. Soc.* **1961**, *83*, 4023.

(2) Grima, J. P.; Choplin, G.; Kaufman, J. *J. Organomet. Chem.* **1977**, *129*, 221.

(3) Antolovic, D.; Davidson, E. R. *J. Am. Chem. Soc.* **1988**, *88*, 3793.

(4) Veillard, A.; Daniel, C.; Rohmer, M.-M. *J. Phys. Chem.* **1990**, *94*, 5556.

(5) Ziegler, T.; Cavallo, L.; Berces, A. *Organometallics* **1993**, *12*, 3586.

(6) Huo, C. F.; Li, Y. W.; Wu, G. S.; Beller, M.; Jiao, H. J. *J. Phys. Chem. A* **2002**, *106* (50), 12161−12169.

(7) Bader, R. F. W., *Atoms in Molecules: A Quantum theory*; Oxford University Press: Oxford, UK, 1990.

(8) Krokidis, X.; Vuilleumier, R.; Borgis, D.; Silvi, B. *Mol. Phys.* **1999**, *96* (2), 265−273.

(9) Krokidis, X.; Noury, S.; Silvi, B. *J. Phys. Chem. A* **1997**, *101* (39), 7277−7282.

(10) Li, X. Y.; Zeng, Y. L.; Meng, L. P.; Zheng, S. J. *J. Phys. Chem. A* **2007**, *111* (8), 1530−1535.

(11) Li, X. Y.; Fan, H. M.; Meng, L. P.; Zeng, Y. L.; Zheng, S. J. *J. Phys. Chem. A* **2007**, *111* (12), 2343−2350.

(12) Zeng, Y. L.; Zheng, S. J.; Meng, L. P. *Inorg. Chem.* **2004**, *43* (17), 5311−5320.

(13) Zeng, Y. L.; Zheng, S. J.; Meng, L. P. *J. Phys. Chem. A* **2004**, *108* (47), 10527−10534.

(14) Zeng, Y. L.; Meng, L. P.; Zheng, S. *J. Mol. Struct.* **2004**, *684* (1−3), 103−110.

(15) Macchi, P.; Sironi, A. *Coord. Chem. Rev.* **2003**, *238*, 383−412.

(16) Malcolm, N. O. J.; Popelier, P. L. A. *J. Phys. Chem. A* **2001**, *105*, 7638−7645.

(17) Polo, V.; Andres, J.; Castillo, R.; Berski, S.; Silvi, B. *Chem.−Eur. J.* **2004**, *10* (20), 5165−5172.

(18) Berski, S.; Andres, J.; Silvi, B.; Domingo, L. R. *J. Phys. Chem. A* **2006**, *110* (51), 13939−13947.

(19) Berski, S.; Andres, J.; Silvi, B.; Domingo, L. R. *J. Phys. Chem. A* **2003**, *107* (31), 6014−6024.

(20) Andres, J.; Berski, S.; Feliz, M.; Llusar, R.; Sensato, F.; Silvi, B. *C. R. Chim.* **2005**, *8* (9−10), 1400−1412.

(21) Balanarayan, P.; Kavathekar, R.; Gadre, S. R. *J. Phys. Chem. A* **2007**, *111*, 2733−2738.

(22) Bader, R. F. W. *J. Phys. Chem. A* **1998**, *102* (37), 7314−7323.

(23) Bader, R. F. W.; Matta, C. F.; Cortés-Guzmán, F. *Organometallics* **2004**, *23* (26), 6253−6263.

(24) Rocha-Rinza, T.; Hernandez-Trujillo, J. *Chem. Phys. Lett.* **2006**, *422* (1−3), 36−40.

(25) Frisch, M. J.; Trucks, G. W.; Schlegel, H. B.; Scuseria, G. E.; Robb, M. A.; Cheeseman, J. R.; Montgomery, J. A., Jr.; Vreven, T.; Kudin, K. N.; Burant, J. C.; Millam, J. M.; Iyengar, S. S.; Tomasi, J.; Barone, V.; Mennucci, B.; Cossi, M.; Scalmani, G.; Rega, N.; Petersson, G. A.; Nakatsuji, H.; Hada, M.; Ehara, M.; Toyota, K.; Fukuda, R.; Hasegawa, J.; Ishida, M.; Nakajima, T.; Honda, Y.; Kitao, O.; Nakai, H.; Klene, M.; Li, X.; Knox, J. E.; Hratchian, H. P.; Cross, J. B.; Bakken, V.; Adamo, C.; Jaramillo, J.; Gomperts, R.; Stratmann, R. E.; Yazyev, O.; Austin, A. J.; Cammi, R.; Pomelli, C.; Ochterski, J. W.; Ayala, P. Y.; Morokuma, K.; Voth, G. A.; Salvador, P.; Dannenberg, J. J.; Zakrzewski, V. G.; Dapprich, S.; Daniels, A. D.; Strain, M. C.; Farkas, O.; Malick, D. K.; Rabuck, A. D.; Raghavachari, K.; Foresman, J. B.; Ortiz, J. V.; Cui, Q.; Baboul, A. G.; Clifford, S.; Cioslowski, J.; Stefanov, B. B.; Liu, G.; Liashenko, A.; Piskorz, P.; Komaromi, I.; Martin, R. L.; Fox, D. J.; Keith, T.; Al-Laham, M. A.; Peng, C. Y.; Nanayakkara, A.; Challacombe, M. G., P. M. W.;; Johnson, B.; Chen, W.; Wong, M. W.; Gonzalez, C.; Pople, J. A. *Gaussian 03*, revision D.01; Gaussian Inc.: Wallingford, CT, 2004.

(26) Keith, T. *AIMAll97 Package*, C1 for Windows; aim@tkgristmill.com: 2006.

(27) Biegler-Konig, F.; Schonbohm, J. *J. Comput. Chem.* **2002**, *23* (15), 1489−1494.

(28) Biegler-König, F. W.; Bader, R. F. W.; Tang, T.-H. *J. Comput. Chem.* **1982**, *3*, 317−328.

(29) Versluis, L.; Ziegler, T.; Fan, L. *Inorg. Chem.* **1990**, *29*, 4530−4536.

(30) Huo, C. F.; Li, Y. W.; Beller, M.; Jiao, H. *Organometallics* **2003**, *22* (23), 4665−4677.

(31) Alagona, G.; Ghio, C.; Lazzaroni, R.; Settambolo, R. *Organometallics* **2001**, *20* (25), 5394−5404.

(32) Luo, X. L.; Tang, D. Y.; Li, M. *Int. J. Quantum Chem.* **2006**, *106* (8), 1844−1852.

(33) Lopez, C. S.; Faza, A. N.; Cossio, F. P.; York, D. M.; de Lera, A. R. *Chem.−Eur. J.***2005**, *11* (6), 1734−1738.

(34) Cortés-Guzmán, F.; Bader, R. F. W. *Coord. Chem. Rev.* **2005**, *249*, 633−662.

(35) Piacenti, F.; Bianchi, M.; Frediani, P.; Menchi, G.; Matteoli, U. *J. Organomet. Chem.* **1991**, *417*, 77−88.